Optimization of the salicylate method for ammonia quantification from nitrogen electroreduction

Juan José Giner-Sanz[1,2], Graham Leverick[3], Valentín Pérez-Herranz[2], Yang Shao-Horn[1,3,4,*]

[1] Research Laboratory of Electronics, Massachusetts Institute of Technology, 77 Massachusetts Avenue, Cambridge, Massachusetts 02139, USA.
[2] IEC group, Depto. Ingeniería Química y Nuclear, Universitat Politècnica de València, Camí de Vera s/n, Valencia 46022, Spain.
[3] Department of Mechanical Engineering, Massachusetts Institute of Technology, 77 Massachusetts Avenue, Cambridge, Massachusetts 02139, USA.
[4] Department of Materials Science and Engineering, Massachusetts Institute of Technology, 77 Massachusetts Avenue, Cambridge, Massachusetts 02139, USA.
[*] Corresponding author:
Y.S.H. - shaohorn@mit.edu

Abstract

The salicylate method is one of the colorimetric methods that is used for ammonia quantification in nitrogen (electro)fixation. While the salicylate method offers advantages in that it avoids working with toxic reagents and does not generate toxic fumes, ammonia quantification is sensitive to the exact experimental conditions (e.g. color development time, exposure to light, etc.) and to a number of interferences (e.g. pH of the samples, presence of interferents, etc.), which leads to reproducibility problems. In this work, the influence of different factors on the ammonia quantification in Nitrogen Reaction Reduction (NRR) using the salicylate method was examined, both in aqueous media and in non-aqueous media. The detailed experimental procedures presented in this work, provide an optimized reference method for quantifying ammonia in NRR screening experiments using the salicylate method.

KEYWORDS: Ammonia quantification, Aqueous samples, Nitrogen reduction reaction, Non-aqueous samples, Salicylate method, UV-visible spectroscopy.

1. Introduction

Ammonia and its derivatives, such as urea, are one of the pillars of modern civilization. Nowadays, these compounds are widely used in the agricultural sector to make synthetic fertilizers [1]. The majority of the world's population relies on food sources enabled by these fertilizers [2-3]. Moreover, ammonia demand is forecasted to increase in the coming years due to the growing global population, as well as ammonia's potential as a renewable energy carrier [4] due to its large hydrogen content (i.e. 17.6 wt.%) [5] and high energy density (4.32 $kWh \cdot L^{-1}$ at -33.3°C and 1 bar) [6].

Today, more than 90% of the annual world production of ammonia is synthetized using the Haber-Bosch process [7]. The development of this industrial process lead to two Nobel Prizes in chemistry: to the industrial chemist Fritz Haber, who developed the process in 1918; and to the chemical engineer Carl Bosch, who scaled up the process in 1931. This century-old process is widely considered as one of the greatest inventions of the 20th century [8-9], and enables ammonia synthesis from molecular nitrogen and hydrogen, using an iron-based catalyst [10]. Unfortunately, the Haber-Bosch process is very energy intensive, consuming between 1% and 2% of the anthropogenic energy [11-13], and is responsible for nearly 1.44% of the total CO_2 emissions [14] since it currently relies on fossil fuels (mainly natural gas) as the source of H_2 [15]. Furthermore, the Haber-Bosch process requires high temperatures (~500°C) and high pressures (>200 atm) [16], which necessitate large centralized ammonia production facilities [17] and makes distributed ammonia production economically unfeasible [18].

Due to these limitations, there is increasing interest in developing alternative technologies to produce ammonia in an environmentally friendly and distributed way [19-20]. Renewable energy-powered electrosynthesis of ammonia from atmospheric nitrogen and water is a promising alternative to the Haber-Bosch process [6, 21]. However, significant improvements in nitrogen reduction reaction (NRR) activity and selectivity are needed [22].

In order to assess candidate NRR catalysts, accurate quantification of the produced ammonia is needed so that the catalyst's ammonia yield rate and faradic efficiency can be determined [23]. Ideally, ammonia quantification should be reliable, cost-effective, easy-to-perform and sensitive, since the produced ammonia concentrations of state-of-the-art NRR catalysts is still low (typically below tens of ppms [24]). Today, several ammonia quantification methods are available, including spectrophotometric (i.e. colorimetric) methods [25-26], ammonia ion-selective based methods [27], ion chromatography [28-29], Fourier transform infrared radiation (FTIR) spectroscopy [30], and ^{1}H NMR spectroscopy [31]. Ammonia has been most extensively quantified using colorimetric methods, such as the Indophenol, salicylate and Nessler methods, due to their low cost, high sensitivity and facile operation [23]. Unfortunately, these colorimetric methods are prone to interferences from impurity ions, nitrogen-containing molecules, and even solvents which hinders their reliability [32-33]. Further experimental difficulty comes from ammonia contamination of samples from the laboratory environment and elements of the experimental setup (e.g. membrane, catalyst, etc…) which can be significant compared to the low concentration of ammonia produced in NRR experiments (in the micromolar, or even nanomolar, range). Contamination of samples with ammonia from non-NRR sources, as well as colorimetric method interferences are responsible for poor reproducibility of reported nitrogen (electro)reduction results [24]. In order

to ensure the reproducibility of NRR experiments, ^{15}N isotopic labelling has been proposed [6, 23-24], where NRR experiments are conducted using $^{15}N_2$. The ^{15}N-enriched ammonia produced by NRR can be distinguished from unenriched ammonia from contamination sources (which is $^{14}NH_3$) providing more rigorous quantification of the ammonia produced from NRR. Unfortunately, ^{15}N isotopic labelling is very expensive, even when the amount of $^{15}N_2$ is reduced by using a closed system [24]. For this reason, colorimetric methods are still used for initial screening of NRR experiments, which then are validated using ^{15}N isotopic labelling. Therefore, minimizing experimental uncertainties during initial NRR screening requires the optimization of colorimetric methods.

The salicylate method is one of the available colorimetric ammonia quantification methods based on the Berthelot reaction. The term "Berthelot reaction" refers to a family of chemical reactions where a phenolic compound reacts with ammonia and a hypochlorite source to form an indophenol-like dye. Marcellin Pierre Eugène Berthelot reported the first example of such reactions in 1859 [34]. These indophenol-like dyes strongly absorb visible light between 630 nm and 720 nm, allowing for ammonia quantification using ultraviolet-visible (UV-Vis) spectroscopy [35], and in situ sensors [36-38]. In the salicylate method, sodium salicylate is used as the phenolic compound, sodium hypochlorite is used as the hypochlorite source, and sodium nitroprusside is added as a catalyst [39]. The salicylate method has the advantage of avoiding toxic reagents [40-41] (such as phenol in the Indophenol method, and mercury salts in the Nessler Method) and also does not generate toxic fumes [42] (such as ortho-chlorophenol produced by the Indophenol method). Unfortunately, the salicylate method is sensitive to the color development time [43] and the exposure to light [42] among many other factors, and has a number of interferences (such as pH [44], nitrogen-containing compounds [45], or transition metal ions [46], etc.) which can lead to errors in the ammonia quantification if not properly accounted for. In order to enhance the reproducibility of the salicylate method, all the relevant parameters that can affect its accuracy and precision should be identified and optimized. While there are some studies, such as Zhao et al. [33] and Zhou and Boyd [47], that address this issue for the Indophenol method and the Nessler method in aqueous media, none exists for the salicylate method in non-aqueous media. In this work, the salicylate method is optimized for ammonia quantification in NRR experiments, in both aqueous and non-aqueous media.

2. Materials and methods

2.1. Materials

Ammonium chloride (Sigma-Aldrich, ACS Grade), ammonia aqueous solution (28-30%, Ensure Millipore, ACS Grade), sodium salicylate (Ensure Millipore, for analysis; and Sigma-Aldrich, ReagentPlus® ≥99.5%), sodium nitroprusside dihydrate (Ensure Millipore, for analysis), sodium citrate dihydrate (Ensure Millipore, for analysis), sodium hydroxide (Sigma-Aldrich, anhydrous, free-flowing pellets ACS reagent), sodium hypochlorite aqueous solution (Sigma-Aldrich, reagent grade, available chlorine 4.00-4.99 %), tetrahydrofuran (Fisher Scientific, 99.9% extra dry, stabilized), ethanol (Sigma-Aldrich, ACS Grade) and lithium perchlorate (Sigma-Aldrich, ACS Grade) were used as received. All the reagents were stored at room temperature, except the sodium hypochlorite aqueous solution, which was stored at 5ºC. Deionized (DI) water was obtained from

a Millipore system (Resistivity: 18.2 MΩ·cm at 25°C; TOC: 4 ppb), and was always freshly prepared just before its use.

The samples were stored and manipulated in scintillation vials (SciLabware, 20 mL). 3 mL disposable methacrylate cuvettes (VWR, 1 cm optical path) were used for UV-Visible measurements. A GENESYS® 180 UV-Visible spectrophotometer was used to measure the UV-Visible spectra.

2.2. The salicylate method for aqueous samples

Today, several variants of the salicylate method can be found in literature. The method used in this work was used in a previous work [46] and was derived from the method originally proposed by Bower and Holm-Hansen [48] and reproduced by Le and Boyd [49].

Three reagent solutions were prepared: the salicylate catalyst solution (S1), the alkaline citrate solution (S2), and the alkaline hypochlorite solution (S3). S1 was prepared by dissolving 2.75 M sodium salicylate and 0.95 mM sodium nitroprusside dihydrate in DI water. S2 was prepared by dissolving 340 mM sodium citrate dihydrate and 465 mM sodium hydroxide in DI water. Finally, S3 was obtained by mixing 10 vol.% of commercial 5% sodium hypochlorite aqueous solution with S2. S1 and S3 were not stored and were always freshly prepared just before analyzing the samples. On the contrary, S2 was prepared in advanced, and stored at room temperature. S1 was kept in an opaque dark bottle during the whole analysis process.

Previous works have reported that the method sensitivity plateaus once a threshold concentration of each one of the reagents (i.e. salicylate ions, hypochlorite ions and nitroprusside ions) is reached [50]. For this reason, the reagent concentration factor (i.e. added volume of each reagent) was not optimized in this work; and instead, the reagent volumes proposed in the original work were used. To analyze a given sample: 5 mL of sample were mixed with 600 µL of S1, and mixed vigorously. Then, in the dark, 1 mL of S3 was added to the aforementioned mixture and again mixed thoroughly. After that, the sample was stored in the dark for 45 minutes, following which its visible spectra was measured using a double beam spectrophotometer. The experimental procedure is summarized in Figure S15. Since the salicylate reagents (especially sodium nitroprusside) have color (Figure S1 and S2), a blank sample was prepared by applying the aforementioned protocol to 5 mL of DI water. This developed blank sample was used as blank and reference sample for the UV-Visible measurement of the different samples. The sample preparation and measurement was done at ambient temperature. All the visible spectra were measured from 850 nm to 350 nm, with a step size of 0.5 nm and a sweep speed of 5 $nm \cdot s^{-1}$.

2.3. The salicylate method for non-aqueous samples

Two strategies have been proposed in literature to apply ammonia quantification methods, based on the Berthelot reaction, to non-aqueous samples. In one method, the reagents are added to the non-aqueous sample directly [51]. Alternatively, the sample is evaporated leaving behind ammonia as salts, which are later redissolved in water and analyzed as though it were an aqueous samples [24]. Although the direct method is simpler, the influence of non-aqueous solvent on the method is not well understood and some non-aqueous solvents are hazardous and must be manipulated in

a fume hood, making it more difficult to prevent interference from light. On the other hand, the evaporation-redissolution method allows for potentially hazardous non-aqueous solvents to be easily evaporated in a fume hood, but adds additional steps (and consequently additional opportunities for error/interference). The evaporation-redissolution method was selected for this work.

To analyze a given batch of non-aqueous samples: the samples were evaporated by placing them uncapped on a hotplate at 50℃ for 15 hours, which allowed the solvent to evaporate completely. The position of the samples on the hotplate was randomized, in order to ortogonalize the position factor from other differentiating factors within the batch of samples (e.g. ammonia concentration, electrolyte, etc.). In this way, in case the position on the hotplate affects significantly the evaporation process, the effect would be randomized (i.e. converted into experimental noise) instead of generating biased results. Once the evaporation was complete, the vials were capped and allowed to cool for 3 hours.

In this work, five different redissolution processes were considered. For redissolution process 1, following cooling, 5 mL of DI water was introduced in each vial, which was then capped, thoroughly shaken and immediately analyzed using the salicylate method presented in section 2.2. For redissolution process 2, 5 mL of DI water was introduced in each vial, which was then capped and thoroughly shaken. Following this, the sample was loaded in a 5 mL syringe, filtered using a 0.22 μm pore size syringe filter (VWR) and immediately analyzed using the salicylate method. For redissolution process 3, 5 mL of DI water was introduced in each vial, which was then capped and thoroughly shaken. The sample was left for 4 days at room temperature, then loaded in a 5 mL syringe, filtered using a 0.22 μm pore size syringe filter (VWR) and immediately analyzed using the salicylate method. For redissolution process 4, 5 mL of DI water was introduced in each vial, which was then capped and thoroughly shaken. The sample was left for 4 days at room temperature and then analyzed using the salicylate method. Finally, for redissolution process 5, 10 mL of DI water was introduced in each vial, which was then capped and thoroughly shaken. The sample was left for 4 days at room temperature and then analyzed using the salicylate method.

The experimental procedure is summarized in Figure S15; and the proposed detailed experimental procedures can be found in the supplementary information, both for aqueous samples (SI section 8.1) and for non-aqueous samples (SI section 8.2).

2.4. Kinetics of color formation and color stability

A parent solution of 0.1 mM Total Ammonia Nitrogen (TAN, i.e. $NH_3 + NH_4^+$), was prepared by dissolving solid NH_4Cl powder in DI water. A set of solutions of different TAN concentrations were prepared by dilution of the parent solution in DI water to yield final sample volumes of 5 mL.

One 20 mL scintillation vial was loaded with 5 mL of one of the NH_4Cl solutions, and another one was loaded with 5 mL of DI water (i.e. blank sample). The salicylate reagents were added to the blank sample, as described in section 2.2; and the resulting mixture was split into two cuvettes: one to serve as a reference sample and the other to blank the UV-Visible spectrophotometer. Once the UV-Visible spectrophotometer was blanked, the same reagent solution additions were done in

the vial containing the NH_4Cl solution, with the only difference, that in this case the S3 addition was performed in the dark. Immediately after adding solution S3 (and starting the chronometer), the content of the vial was loaded into a disposable methacrylate cuvette, and the UV-Visible spectrum was measured at different times. In one set of experiments, the UV-Visible spectra were measured from 850 nm to 350 nm, with a step size of 0.5 nm, at the maximum sweep speed allowed by the GENESYS® 180 UV-Vis instrument (i.e. 20 $nm \cdot s^{-1}$) in order to minimize the change of the spectrum during the measurement itself. In another set of experiments, the absorbance at only 652 nm (i.e. indophenol-type dye peak) was measured every 30 seconds.

To assess the color stability, the whole batch of samples analyzed in the color formation experiments were stored and measured at different times, over a period of around one month. When not being measured, the samples were stored in the dark. The sample spectra were always measured in the same order the reagents had been added to the samples, using the same blank sample as blank and reference for all the measurements. All the visible spectra were measured from 850 nm to 350 nm, with a step size of 0.5 nm and a sweep speed of 5 $nm \cdot s^{-1}$.

2.5. pH dependence experiments

Calibration samples (with different TAN concentrations) were prepared in different electrolytes: in water, in H_2SO_4 solutions with different H_2SO_4 concentrations, and in KOH solutions with different KOH concentrations. In this way, calibration sets of samples of different TAN concentrations, at different pHs, were obtained. The experimental procedure to prepare and measure the calibration samples was exactly the same as described in sections 2.2 and 2.4; with the only difference that instead of using DI water to prepare the NH_4Cl parent solution and its corresponding dilutions, the corresponding electrolyte was used for this matter in each case.

2.6. Reproducibility of the ammonia quantification

In order to assess the reproducibility of the method, the aqueous and non-aqueous absorbance-TAN concentration calibration curves were obtained on several different days. In order to obtain these calibration curves, a set of aqueous (or non-aqueous) calibration samples were prepared by successive dilutions of a mother solution of known TAN concentration. In the case of aqueous samples, the mother solution was prepared by dissolving solid NH_4Cl powder in DI water; whereas, for the non-aqueous calibration samples, the mother solution was prepared by mixing commercial 28-30% ammonia aqueous solution with the non-aqueous electrolyte (i.e. Tetrahydrofuran-ethanol 99:1 vol.%, 0.2M $LiClO_4$). A different TAN standard had to be used for the non-aqueous samples, due to the limited solubility of NH_4Cl in Tetrahydrofuran (THF). Since the ammonia aqueous solution is not a primary standard (i.e. its TAN concentration is not exactly known, and may change with time), it was normalized prior to preparing each calibration sets of non-aqueous samples. The normalization was performed using the salicylate method for aqueous samples (section 2.2). Once the calibration samples were ready, the aqueous ones were analyzed using the salicylate method for aqueous samples (section 2.2), while the non-aqueous ones were analyzed using the salicylate method for non-aqueous samples (section 2.3).

For the aqueous samples, in addition to the reproducibility in different days, the reproducibility due to the use of different reagents was also analyzed. In this case, two commercial sodium

salicylate reagents (Ensure Millipore, for analysis; and Sigma-Aldrich, ReagentPlus® ≥99.5%) were tested.

3. Results and Discussion

3.1. The kinetics of the indophenol dye formation in aqueous solutions

Immediately upon the addition of the salicylate reagents to a 0.1 mM Total Ammonia Nitrogen (TAN, i.e. $NH_3 + NH_4^+$) sample (Figure 1.a.), the absorbance of the reacting mixture against the blank sample (salicylate reagents added to DI water without ammonia) was found to be about 0 at every wavelength. The initial color of the mixture is thus independent of the ammonia concentration in the sample, and is determined by the color of the salicylate reagents (SI section 1). Two minutes after adding the reagents, the sample spectrum had barely changed, showing that there is an initiation time, on the order of minutes, between adding the reagents and the onset of color formation in the mixture. After a few minutes, the color started to change as suggested by the appearance, and subsequent growth, of a Gaussian peak centered around 652 nm. This peak can be assigned to the formation of an indophenol-type dye during the salicylate reaction [52]: $NH_3 + OCl^- + 2C_7H_5O_3^- \rightarrow$ Indophenol dye. The peak maximum increased with time, while the peak position remained constant throughout the whole color development. This observation suggests that the reaction intermediates do not absorb UV-Visible light, and therefore the peak growth is only due to the indophenol dye concentration build up in the mixture. In addition to the main peak, a secondary feature with significantly lower absorbance, developed in the low wavelength range (below 400 nm). This secondary feature can also be attributed to the dye, and not to reaction intermediates, since it does not decay with time (in the reaction time scale). After around 30 minutes, the spectrum reached steady state, indicating that all the ammonia in the sample had been converted into the Indophenol-type dye. The steady-state spectrum consisted of a major wide Gaussian peak at 652 nm (Full Width at Half Maximum, FWHM, of around 115 nm) and a secondary feature around 370 nm. No significant difference was observed for times ranging from 30 to 90 minutes, indicating that the dye was stable for at least an hour after reaching steady-state (See section 3.2).

The 652 nm absorbance of both 0.1 mM and 10 μM TAN samples increased with time following a logistic curve with time delay (Figure 1.b.). The 0.1 mM TAN sample displayed a shorter time delay than the 10 μM TAN sample (inset of Figure 1.c). A shorter delay with higher ammonia concentration is consistent with faster buildup of reaction intermediates in samples with higher ammonia concentrations (Figure S7). Following the initial time delay, the peak absorbance was found to increase exponentially, until an inflection point was reached. After the inflection point, the absorbance followed an asymptotic exponential growth, tending to a steady state value. The steady-state 652 nm absorbance was proportional to the initial ammonia concentration in the sample (Figure S4), reaching 1.780 and 0.178 for the 0.1 mM TAN and 10 μM TAN samples, respectively. The observed time evolution displays the characteristic the s-shaped curve of the logistic model and is consistent with the reaction mechanism proposed by Krom [53] (Figure S5):

$$NH_3 + OCl^- \rightarrow NH_2Cl + OH^- \quad \text{(R1)}$$

$$C_7H_5O_3^- + NH_2Cl \rightarrow C_7H_4O_3NH_2^- + Cl^- + H^+ \quad \text{(R2)}$$

$$C_7H_4O_3NH_2^- \xrightarrow{[Fe(CN)_5NO]^{2-}} C_7H_3O_3NH^- + H_2 \quad \text{(R3)}$$

$$C_7H_5O_3^- + C_7H_3O_3NH^- \rightarrow [C_7H_4O_3NC_7H_3O_3]^{2-} + H_2 \qquad \text{(R4)}$$

Given the sample pH>12 following addition of the alkaline hypochlorite reagent (Figure 3c) and the pKa of ammonium ions (9.25), hypochlorous acid (7.53) and salicylic acid (2.97) [54], at the beginning of the reaction, these species are in their NH_3, OCl^- and salicylate forms, respectively. Krom's mechanism consists of 4 reactions in series (Figure S5). The reaction begins with the formation of monochloramine from ammonia and the hypochlorite ion. Next, monochloramine reacts with salicylate to form 5-aminosalicylate. Then, 5-aminosalicylate is oxidized, which is catalyzed by sodium nitroprusside. Finally, the oxidized 5-aminosalicylate combines with a second salicylate ion via oxidative coupling to form the indophenol dye. With the reagent concentrations present in the salicylate method (section 2.2), ammonia is the limiting reagent, whereas sodium salicylate and sodium hypochlorite are in large excess. Therefore, the concentrations of sodium salicylate and sodium hypochlorite remain roughly constant during the dye formation reaction. The monochloramine formation step (reaction R1) is known to be extremely fast [55-56]. Consequently when the alkaline hypochlorite reagent (S3) is added to the sample, all the ammonia in the mixture is converted instantaneously (i.e. at t = 0) into monochloramine. After that, the reaction intermediates ($C_7H_4O_3NH_2^-$ and $C_7H_3O_3NH^-$) are formed and then consumed, until all the ammonia has been converted into indophenol dye (Figure S7). Fitting a kinetic model to the time-dependent 652 nm absorbance signal suggests that the oxidation of 5-aminosalicylate (reaction R3) is the rate-limiting step, which is consistent with the requirement of a catalyst (sodium nitroprusside) for this step (Table S1).

The fitted kinetic model was used to calculate the relative error in the ammonia concentration quantification as a function of the TAN concentration in the sample and the time after the addition of reagent S3 to the sample at which the absorbance of the sample is measured (Figure 1.d). The relative error in the ammonia concentration quantification (e, in %) can be defined as:

$$e = \frac{C_{TAN}^{Measured} - C_{TAN}^{Sample}}{C_{TAN}^{Sample}} \cdot 100 \qquad (1)$$

Where C_{TAN}^{Sample} corresponds to the real TAN concentration in the sample, and $C_{TAN}^{Measured}$ denotes the TAN concentration measured using the salicylate method. The color saturation time is taken as the time it takes for the 652 nm absorbance to reach 99.5% of its steady state value (i.e. 0.5% relative error). The color saturation time depends on the TAN concentration of the sample: samples with higher TAN concentrations display a lower color saturation time. For samples with TAN concentrations in the 0-0.16 mM range, the color saturation time varies from 20 to 32 minutes (Figure 1.d). In order to ensure reliable results, we recommend that UV-Vis spectra should be measured 45 minutes after the addition of the salicylate reagents to the samples, to ensure the dye formation reaction is complete.

After reaching the steady-state peak absorbance, the absorbance remained relatively constant for at least an hour. For spectra taken 1 and 2 hours after the reaction, the peak absorbance only decreased by 0.6% for the 0.1 mM TAN sample, and did not decrease at all for the 10 µM TAN sample (Figure 1.b). Since development time differences in the order of minutes do not lead to significant errors in the measurement after the initial dye formation reaction is complete, no special

care needs to be taken to ensure that all the samples have exactly the same development times enabling analysis of samples in moderately sized batches.

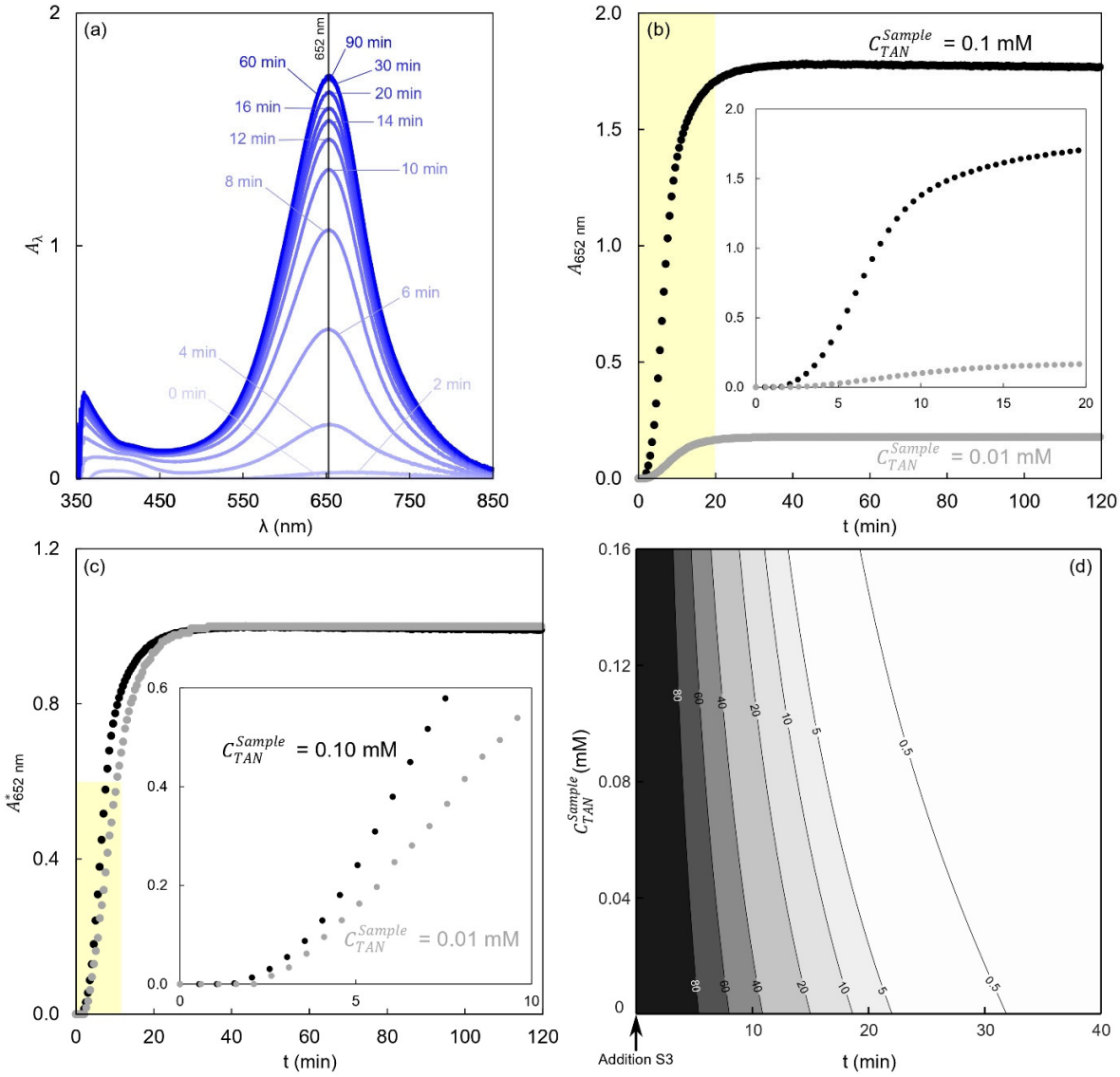

Figure 1. Time evolution of the (a) UV-Visible spectrum (i.e. absorbance, A_λ, as a function of the wavelength λ) and the (b) absorbance at 652 nm, of a 0.1 mM TAN concentration sample after the addition of the salicylate reagents (i.e. $t = 0$ corresponds to the addition of reagent S3 to the sample). The UV-Visible spectra (a) were measured against the reference sample (i.e. blank sample analyzed by the salicylate method), from 850 nm to 350 nm, with a step size of 0.5 nm, at the maximum sweep speed of the instrument (i.e. 20 nm·s^{-1}). The absorbance at 652 nm (b) was followed by measuring the absorbance at the selected wavelength (i.e. individual wavelength absorbance measurement) with a sampling period of 30 seconds. This wavelength was selected since it was identified as the wavelength at which the Indophenol-type dye absorbs the most (i.e. wavelength of the peak maximum) in the (left) subfigure. In addition to the curve of the 0.1 mM TAN concentration sample (black points), the curve of the 0.01 mM TAN concentration sample (gray points) is presented as well. The inset diaplays the zoom for times below 20 minutes (yellow region). (c) Time evolution of the normalized absorbance at 652 nm (i.e. $A^*_{652\ nm}$) of the 0.1 mM TAN and 0.01 mM TAN samples after the addition of the salicylate reagents. The normalized absorbance was calculated dividing the absorbance at 652 nm (a) by the maximum absorbance ay 652 nm of each sample. The inset displays the zoom for times below 10

minutes (yellow region). (d) Relative error (e, expressed in %) in the ammonia concentration quantification as a function of the TAN concentration in the sample and the time at which the absorbance of the sample is measured. The time origin corresponds to the addition of reagent S3 to the sample. The relative errors were calculated using the kinetic models proposed in this work for the dye formation (SI section 3) and the dye decomposition (SI section 4).

3.2. Instability of the indophenol dye in aqueous solutions

Over the hour time scale, the characteristic dye peak (~652 nm) was found to decay with time while the absorbance at wavelengths below 500 nm did not change significantly (Figure 2.a), during which the sample switched from its initial characteristic blue to a final deep red color (Figure S8). This change can be attributed to the decomposition of the indophenol-type blue dye, which is not stable; and the formation of decomposition products, some of which present(s) a red coloration [50]. This is consistent with previous works that report that indophenol-type dyes are only stable for 4 to 6 hours [57-58], although stability can be extended to 24 hours and longer if the solutions are protected from carbon dioxide absorption and direct sunlight [59].

For 0.01 mM to 0.1 mM TAN samples, the absorbance at 652 nm decreased linearly with time for the first ~170 hours (Figure 2.c), where the slope of the linear decay was observed to increase with increasing ammonia concentration of the initial sample. For times >170 hours, the linear trend transformed to asymptotic exponential (Figure 2.b). This time evolution is inconsistent with a potential rate-law kinetic model (Figure S9). The inconsistency of the dye decomposition rate with an exponential decay suggests that the decomposition mechanism is more complex than a spontaneous decay of the dye into its decomposition products. The dye decomposition rate is consistent with a Laidler kinetic model for all the initial dye concentrations (Figure S10.a). This is consistent with a two-step decomposition mechanism: a first fast equilibrium step (that could correspond with the oxygen solubility equilibrium), and a second irreversible step (that could be the dye oxidation by oxygen). However, although the Laidler model is able to accurately reproduce the dye concentration decay for all of the samples, the kinetic parameters depend significantly on the initial dye concentration (Figure S10.b). Several hypotheses can explain this dependence. The positive dependence of the kinetic parameters on the initial dye concentration could be due to the existence of at least one reaction in parallel with the dye decomposition reaction that also involves whatever compound reacts with the dye during its decomposition (e.g. oxygen), and at least one of the reagents of the salicylate reaction. For low initial dye concentrations, the excess of salicylate reagents is greater, and consequently the parallel reaction dominates on the dye decomposition reaction, leading to lower dye decomposition rates. On the contrary, for large initial dye concentrations, the excess of salicylate reagents is lower, and consequently the dye decomposition reaction dominates on the parallel reaction, leading to higher dye decomposition rates. However, this hypothesis is unlikely since the salicylate reagents are in great excess with respect to ammonia, and therefore the variation of the excess of salicylate reagents with the initial dye concentration is quite limited. Another possible hypothesis for explaining the dependency observed experimentally is that the dye could be an autocatalyst of its own decomposition reaction. Alternatively, maybe one or more of the decomposition products catalyze the decomposition reaction.

The relative error for ammonia quantification using the salicylate method due to dye decomposition was estimated from the fitted Laidler kinetic model as a function of the TAN concentration and sample storage time (Figure 2.d). The time decay of the dye implies that the analyzed samples have an expiry date once the reagents have been added (even when kept in the

dark). For instance, the measurement error for a 0.1 mM TAN concentration sample is of only 0.8%, 6 hours after the reagent addition, but it grows to 5.8%, 1 day after the reagent addition and it is more than 95%, 1 month later. This expiry time can be defined as the time at which the measurement error due to the dye decay reaches a certain maximum permissible value. The expiry time of a given sample will depend on its TAN concentration and on the selected maximum measurement error (Figure S11). For example, for a 0.1 mM TAN sample, if the maximum measurement error is 5% then the sample must be measured within 17 hours after adding the reagents. Therefore, to prevent errors due to dye decomposition, it is recommended that samples are measured within 5 hours of adding the reagents.

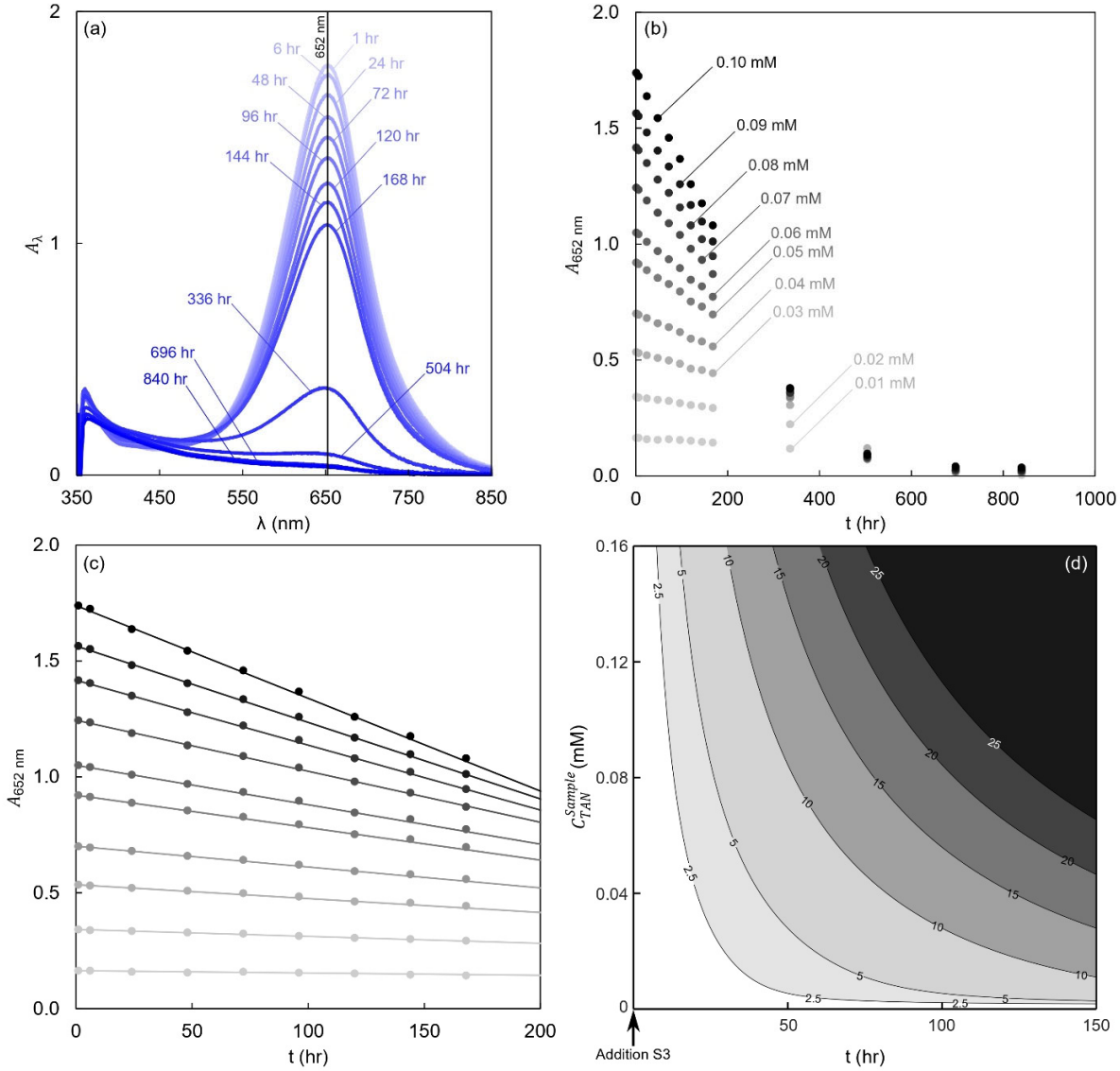

Figure 2. (a) Time stability of the UV-Visible spectrum (i.e. absorbance, A_λ, as a function of the wavelength λ) of a 0.1 mM TAN concentration sample analyzed using the salicylate method. The 1 hr spectrum from this figure corresponds to the 60 min spectrum of figure 1.a. All the UV-Visible spectra were measured against the reference sample (i.e. blank sample analyzed by the salicylate method), from 850 nm to 350 nm, with a step size of 0.5 nm, at a sweep speed of 5 nm·s^{-1}. Between measurements all the samples were kept in a dark place. (b) Time stability of the

652 nm absorbance of samples of different TAN concentrations after beeing analyzed by the salicylate method. The absorbance at 652 nm represented here, was obtained from the corresponding UV-Visible spectrum, for instance the black points (i.e. 0.10 mM TAN) correspond to the peak maximum of the spectra in the (a) subfigure. The inset displays the zoom for times greater than 200 hours (yellow region). (c) Zoom for times below 200 hours. The lines correspond to the fitted linear regression lines (R^2 is greater than 99.95% in all cases). (d) Relative error (e, expressed in %) in the ammonia concentration quantification as a function of the TAN concentration in the sample and the time at which the absorbance of the sample is measured. The time origin corresponds to the addition of reagent S3 to the sample. The relative errors were calculated using the kinetic models proposed in this work for the dye formation (SI section 3) and the dye decomposition (SI section 4). This figure is the continuation of figure 1.d. for larger times, in the hour order of magnitude instead of the minute order of magnitude (figure 1.d. would be squezzed into the vertical axis of (d)).

3.3. Effect of the sample pH on the ammonia quantification in aqueous solutions

In DI water and in 0.1 M KOH, the salicylate method produced the characteristic blue gradation with TAN concentration (Figure S13). However, in 0.1 M H_2SO_4, no blue color was formed and instead a white solid precipitated after the addition of the salicylate catalyst reagent (S1) to the sample. This precipitate remained after the addition of S3 and no color developed, leading to a pale yellow solution with a white precipitate at the bottom (Figure S13). When an excess of NaOH was added to the mixture, the precipitate redissolved, confirming that precipitation upon the addition of S1 was caused by the low pH of the H_2SO_4 solution. This precipitate is attributed to salicylic acid that can form when the salicylate catalyst reagent (S1) is added to a solution with pH below the pKa of the salicylic acid-salicylate acid-base pair (2.97) [54]. The solubility of salicylic acid is 2.48 $g \cdot L^{-1}$/18 mM [54] which is much lower than that of sodium salicylate (1.24 $kg \cdot L^{-1}$/7.7 M [54]) and is also lower than the concentration of salicylic acid/salicylate following the addition of S1 to the solution (250 mM). The precipitation of salicylic acid from the solution greatly reduces the availability of salicylate ions, impairing the dye formation reaction (Figure S5) and explaining the absence of blue color in the 0.1 M H_2SO_4 samples.

The absorbance-TAN concentration calibration curves obtained in water, in KOH, and in 100 nM H_2SO_4 were all equivalent within experimental error (Figures 3.a and 3.b). However, in 10 μM H_2SO_4, the effective molar attenuation coefficient (14.8 $mM^{-1} \cdot cm^{-1}$) was significantly lower than that of water (17.7 $mM^{-1} \cdot cm^{-1}$). Moreover, in 1 mM and 0.1 M H_2SO_4 the obtained calibration curves were nearly flat, consistent with negligible dye formation. Reduced effective molar attenuation coefficients were associated with a lower pH of the sample, as well as the solution after adding salicylate reagents (Figure 3.c). In water, KOH and 100 nM H_2SO_4, both the pH after the addition of the salicylate reagents and the obtained calibration curves were equivalent within experimental error. On the other hand, for 10 μM, 1 mM and 0.1 M H_2SO_4, the reaction pH was lower than in the water case and there was a resulting deviation in the obtained calibration curves. It is a well-known fact that the salicylate reaction is highly sensitive to the pH [50, 60]. For instance, Krom observed a significant reduction of the peak absorbance (i.e. nearly halved) when the dye is formed at pH 10 in comparison to when the dye formation reaction takes place at pH 12 [53]. Consequently, the lower effective molar attenuation coefficient of the calibration curve of the 10 μM solution is attributed to the dye formation reaction occurring at too low pH, leading to impaired dye formation. In the 1 mM and 0.1 M H2SO4 solutions, salicylic acid also precipitated out of the solution due to the pH being below the pKa of the salicylic acid-salicylate acid-base pair upon addition of reagent S1, leading to reduced availability of salicylate ions and further reducing the dye yield such that dye formation was negligible.

The salicylate method described in section 2.2. (Figure S15), works properly for samples in the 6.50 to 13.00 pH range. For these samples, there is no salicylic acid precipitation upon the addition of reagent S1, and the addition of S3 reagent raises the pH to the optimum reaction pH, leading to calibration curves that are invariant with respect to sample pH. For samples with initial pHs between 4.00 and 6.50, while there is no salicylic acid precipitation upon the addition of reagent S1, the addition of reagent S3 is unable to increase the pH to its optimum value, which causes a significant effect on the effective molar attenuation coefficient (and therefore, on the ammonia quantification). Finally, for samples with pHs below 4.00, the salicylate precipitates out of the solution as salicylic acid upon the addition of reagent S1, nearly completely inhibiting the color formation. Reagent S3 should never be added to a sample in which salicylic acid has precipitated; since this is an indicator of low pH, and adding S3 to a low pH sample produces toxic gases. Samples with pHs below 6.50 should be neutralized with NaOH prior to applying the salicylate method (being sure to correct the obtained results for the dilution effect due to NaOH addition).

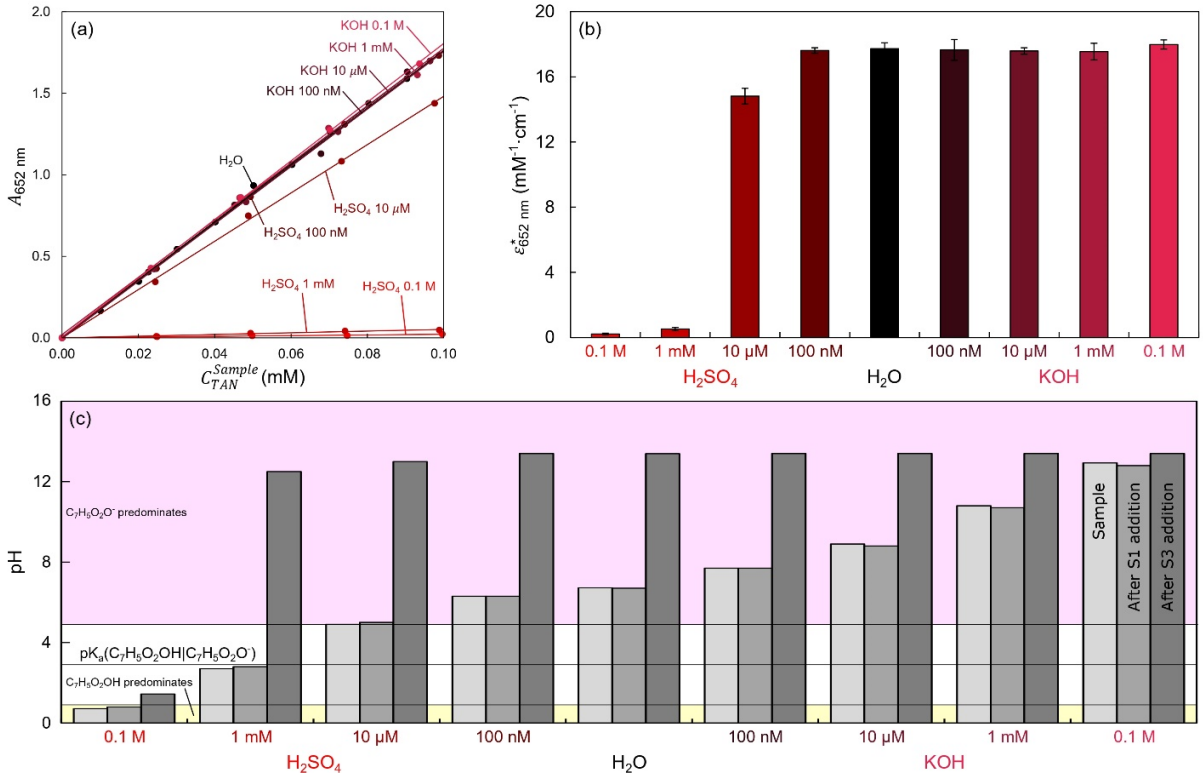

Figure 3. (a) The 652 nm peak calibration curves obtained for samples in different solutions (i.e. different pHs). These curves were obtained by representing the absorbance at 652 nm ($A_{652\ nm}$) as a function of the TAN concentration in the sample (C_{TAN}^{Sample}) for the different samples, after analyzing them using the salicylate method for aqueous samples (section 2.2 and Figure S15). The dots correspond with the experimental points, while the lines are the fitted linear regression lines. From the slopes of the fitted lines, and the optic path of the used cuvettes (l=1cm), the effective molar attenuation coefficient ($\varepsilon^{\star}_{652\ nm}$) was determined for each solution (b). The two-sigma error bars are displayed on the figure. (c) The pH of the sample before any addition, after adding reagent S1 and after adding reagent S3, for each one of the different solutions. The black dotted line marks the pKa of the salicylic acid-salicylate pair, while the red dotted lines identify the salicylic acid and salicylate predominance regions.

3.4. Reproducibility of the ammonia quantification method in aqueous samples

652 nm peak absorbance-TAN concentration calibration curves obtained on different days with two different reagent brands form two distinct clusters (Figure 4.a): all points for brand 1 (independent of the day measured) fall on the same line, whereas all points for brand 2 (independent of the day measured) fall on a different line. This indicates that calibration curves obtained with the same brand reagents were very reproducible when repeated on different days, but the calibration curve is sensitive to the brand of reagents used. Further support comes from the experimental effective molar attenuation coefficients obtained by linear fitting of the different experimental calibration curves (Figure 4.b). A statistical analysis of variance (ANOVA) of the effective molar attenuation coefficients (SI section 6) showed that the reagent brand factor had a statistically significant effect ($p<0.0001$) while the day the calibration curves was obtained on did not ($p>0.05$). Therefore, a calibration curve from a previous day can reliably be applied to samples analyzed on a different day, provided the reagents used are kept consistent. However, in case of changing the reagent, a new calibration curve should be obtained. Although no differences were observed in this work between different lots of a given reagent, it is advisable to obtain a new calibration curve when starting a new reagent lot, even if it is from the same supplier and brand. Even though it is not strictly necessary to include a calibration set in every batch of analyzed samples when working with the same reagent, doing so can still be advantageous. These calibration samples can be used to validate the results from a batch of analyzed samples, allowing for the detection of any errors that may occur during salicylate analysis.

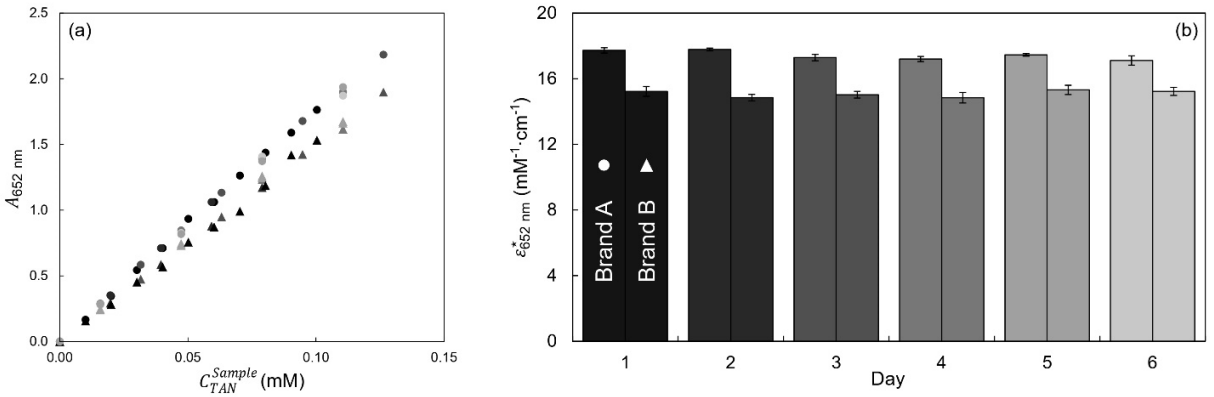

Figure 4. (a) The 652 nm peak calibration curves obtained for aqueous samples in different days (i.e. each day corresponds to a different color), using comercial sodium salicylate from two different brands (circles: brand 1; triangles: brand 2). These curves were obtained by representing the absorbance at 652 nm ($A_{652\,nm}$) as a function of the TAN concentration in the sample (C_{TAN}^{Sample}) for the different samples after analyzing them using the salicylate method for aqueous samples (section 2.2 and figure S15). From the slopes of the fitted linear regression models, and the optic path of the used cuvettes (l=1cm), the effective molar attenuation coefficient ($\varepsilon^{\star}_{652\,nm}$) was determined for each day and reagent brand (b). The two-sigma confidence level error bars of the effective molar attenuation coefficient are displayed on the figure.

3.5. Effect of the evaporation process on the quantification of non-aqueous samples

In this work, the non-aqueous electrolyte used by Tsuneto and coworkers [61] (i.e. Tetrahydrofuran-ethanol 99:1 vol.%, 0.2 M $LiClO_4$) was selected as the non-aqueous media example. This selection was due to the fact that Tsuneto's work is one of the only works in electrochemical NRR that has been reproduced in a recent study [24], and therefore it corresponds to one of the most promising electrolytes in the state-of-the-art non-aqueous NRR field.

Absorbance-TAN concentration calibration curves were obtained for 4 sets of non-aqueous samples based on the non-aqueous electrolyte used by Tsuneto and coworkers [61]: (1) THF-ethanol 99:1 vol.%; (2) THF-ethanol 99:1 vol.% 0.2 M $LiClO_4$; (3) THF-ethanol 99:1 vol.% to which 250 µL of concentrated HCl was added prior to evaporation and (4) THF-ethanol 99:1 vol.% 0.2 M $LiClO_4$ + 250 µL HCl (Figure 5.a). In all cases, the obtained calibration curve had high linearity (R^2>0.95). The fact that the evaporation-redissolution process did not affect to the linearity of the obtained calibration curve implies that the losses have a multiplicative effect on the final maximum absorbance with a loss coefficient that is independent of the ammonia concentration. Therefore, the effective molar attenuation coefficient after loss i, $\varepsilon_i^\star(\lambda_{max})$, can be expressed in terms of the effective molar attenuation coefficient in aqueous samples, $\varepsilon_{H_2O}^\star(652\ nm)$; and a loss factor, η_i:

$$\varepsilon_i^\star(\lambda_{max}) = (1-\eta_i)\cdot\varepsilon_{H_2O}^\star(652\ nm) \tag{2}$$

The loss factor for a given process can be broken down into the individual loss factors of the different losses that occur in that process:

$$\eta_i = 1 - \prod_{j\in\{\text{losses in process i}\}} (1-\eta_j) \tag{3}$$

The evaporation-redissolution process loss factors can be calculated by dividing the effective molar attenuation coefficient by the effective molar attenuation coefficient in aqueous samples (Figure 5.b), and applying equations (2) and (3).

The evaporation-redissolution process loss factor in the case of the THF-ethanol 99:1 vol.% samples was $\eta_{eva-red}^{THF+EtOH} \approx 0.94$, indicating that the losses associated with the evaporation-redissolution process were very large when no HCl was added prior to evaporation. This high loss factor is attributed to the form in which ammonia is in these samples: when no HCl is added to the samples, ammonia is mostly in its NH_3 form, which has a vapor pressure of 20.32 bar at 50ºC [62], leading to significant evaporation. Adding 250 µL of concentrated HCl prior to evaporation reduced the loss factor to $\eta_{eva-red}^{THF+EtOH+HCl} \approx 0.32$ which is attributed to an increased proportion of TAN existing as NH_4^+ following HCl addition, whereNH_4^+ does not readily evaporate. Although HCl addition reduces the TAN lost to evaporation, the >30% loss factor is still significant and needs to be carefully considered when analyzing non-aqueous samples.

Varying the amount of HCl added prior to evaporation resulted in a volcano trend, where the maximum absorbance (lowest loss factor) was obtained when 250 µL of concentrated HCl was added (Figure 6). For HCl <250 µL, increasing the volume of HCl increased the peak maximum absorbance (i.e. reduced the loss factor), where a large increase was observed moving from "no acid" (i.e. 0 µL) to 20 µL, followed by a shallower, roughly linear increase up to the maximum at 250 µL. Decreasing loss factor with increasing HCl volume is attributed to a higher fraction of the ammonia being in NH_4^+ form when more HCl is added to the sample. Samples with 500 µL and 1000 µL HCl showed a decrease in peak maximum absorbance that was roughly linear with the amount of HCl (Figure 6). Increasing loss factor with increasing HCl volume is attributed to decreasing pH of the redissolved sample from 7.6 (0 µL HCl), to 5.6 (250 µL HCl), to 5.5 (1000 µL HCl) (Table S3), which reduces the dye yield as demonstrated in section 3.3. Although increasing HCl lowers the pH of the redissolved sample, the pH is significantly higher than directly adding the HCl to an aqueous sample (Table S3), indicating that most of the HCl is removed by the evaporation process. The competing effects of decreasing TAN evaporation, but also decreasing dye yield with increasing volumes of add HCl gives rise to an optimum HCl volume of 250 µL. This optimum value was found to be very sensitive to the exact evaporation procedure (e.g. position of the hotplate, air circulation in the zone, exact thermal gradients in the vials, etc…), and slight changes led to different values of optimum HCl volume (Figure S20).

The presence of $LiClO_4$ in the samples resulted in additional losses of $\eta_{LiClO_4}^{THF+EtOH+LiClO_4} \approx 0.20$ and $\eta_{LiClO_4}^{THF+EtOH+LiClO_4+HCl} \approx 0.38$, which were obtained by comparing the losses with and without $LiClO_4$ with all other variables held constant. In order to assess whether the negative interference from $LiClO_4$ occurs during the dye formation process (i.e. dye production yield) or due to coordination with the indophenol dye (i.e. intrinsic molar attenuation coefficient), the dye formation reaction was carried out in aqueous samples without $LiClO_4$ and then $LiClO_4$ was added immediately prior to measuring UV-Vis spectra (Figure S17.a). The resulting UV-Vis spectra showed comparable interference from $LiClO_4$ when it was added after the dye formation as compared to when it was present during the dye formation reaction (Figure S17.b) indicating that the negative interference from $LiClO_4$ in aqueous samples is due to coordination with the dye that alters its intrinsic molar attenuation coefficient, while the dye production yield remains unchanged. LiTFSI presents a similar interference effect to $LiClO_4$ (Figure S18), which suggests that Li^+ ions are responsible of the negative interference on the salicylate method.

The loss factor associated with $LiClO_4$ was larger in non-aqueous samples that went through the evaporation-redissolution process ($\eta_{LiClO_4}^{THF+EtOH+LiClO_4} \approx 0.20$ and $\eta_{LiClO_4}^{THF+EtOH+LiClO_4+HCl} \approx 0.38$) than for aqueous samples that did not ($\eta_{LiClO_4}^{H_2O} \approx 0.12$), suggesting that $LiClO_4$ also influences the evaporation-redissolution process (Figure S17). In samples with no HCl added, $LiClO_4$ increased the resulting maximum absorbance, suggesting less TAN lost to evaporation, which is attributed to co-crystallization of TAN and $LiClO_4$ (Figures S18 and S19). However, in samples with HCl added, the maximum absorbance decreased with $LiClO_4$ addition, consistent with a larger loss factor. This larger loss fator is attributed to lower dye yield caused by the accompanying decrease in the pH of the redissolved samples from ~5.5 without $LiClO_4$ to ~2.4 with $LiClO_4$ (Table S3).

Decreasing pH of redissolved samples with LiClO4 is attributed to co-crystalization of HCl and $LiClO_4$ which reduces the amount of HCl lost to evaporation.
The evaporation-redissolution process introduces significant losses to the method, even when HCl is added to the samples before evaporating them. The main practical implication of this observation is that an aqueous calibration curve cannot be applied to non-aqueous samples and that a non-aqueous calibration curve has to be obtained where the electrolyte composition and evaporation conditions are carefully matched to the samples to be analyzed. Depending on the non-aqueous solvent used, the low solubility of NH_4Cl may necessitate the use of an aqueous secondary standard solution that requires an extra standardization process, although ammonium salts with other counter anions such as NO_3^- that might be more soluble may also serve as a standard. Losses in the evaporation-redissolution process also reduce the sensitivity of the salicylate method from 60 nM for aqueous samples (Figure S4) to 135 nM for the non-aqueous THF-based samples considered in this work.

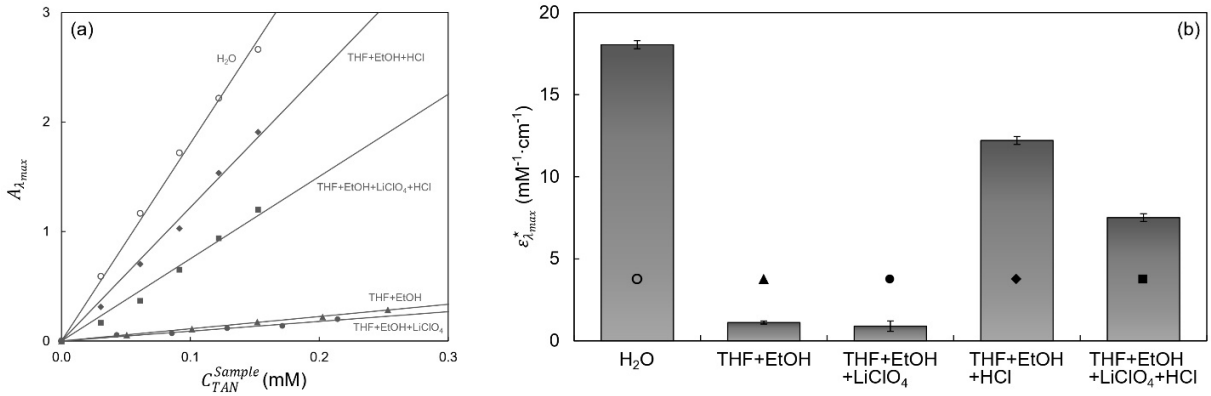

Figure 5. (a) The calibration curves obtained for samples in different electrolytes: H_2O, water; THF+EtOH, THF-ethanol 99:1 vol.%; THF+EtOH+$LiClO_4$, THF-ethanol 99:1 vol.% 0.2 M $LiClO_4$; THF+EtOH+HCl, THF-ethanol 99:1 vol.% to which 250 µL of concentrated HCl (37 %) were added prior to evaporation; THF+EtOH+$LiClO_4$+HCl, THF-ethanol 99:1 vol.% 0.2 M $LiClO_4$ to which 250 µL of concentrated HCl (37 %) were added prior to evaporation. These curves were obtained by representing the maximum absorbance ($A_{\lambda_{max}}$) as a function of the TAN concentration in the original non-aqueous sample (C_{TAN}^{Sample}) for the different samples after analyzing them using the salicylate method for non-aqueous samples (section 2.3 and figure S15) for all the sets of samples, with the exception of the H_2O set, which was analyzed using the salicylate method for aqueous samples (section 2.2 and figure S15). These calibration curves are based on the maximum absorbance, instead of the absorbance at 652 nm, because some of the samples present an hypsochromic shift (Figure S16). The dots correspond with the experimental points, while the lines are the fitted linear regression lines. From the slopes of the fitted linear regression models, and the optic path of the used cuvettes (l=1cm), the effective molar attenuation coefficient ($\varepsilon^{\star}_{652\,nm}$) was determined for each set of calibration samples (b). The two-sigma error bars are displayed on the figure.

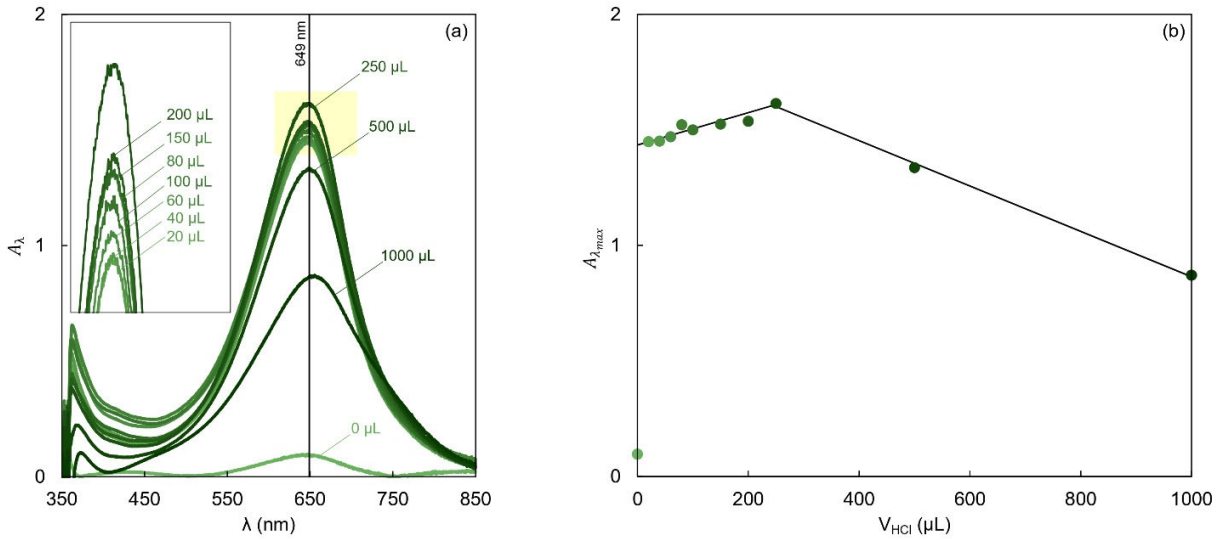

Figure 6. (a) UV-Visible spectra (i.e. absorbance, A_λ, as a function of the wavelength λ) obtained when the salicylate method for non-aqueous samples (section 2.3 and figure S15) was applied to THF-ethanol 99:1 vol.% 0.2 M LiClO4 samples of a given TAN concentration, after the addition of different volumes of concentrated HCl (37 %) prior to the evaporation process. All the UV-Visible spectra were measured against the reference sample (i.e. blank sample analyzed by the salicylate method), from 850 nm to 350 nm, with a step size of 0.5 nm, at a sweep speed of 5 nm·s^{-1}. The inset shows the detail of the spectra highlighted in gray. (b) The maximum absorbance ($A_{\lambda_{max}}$) of the spectra (i.e. peak height in the (a) subfigure) as a function of the HCl volume added before evaporation. The dots correspond with the experimental points, while the lines just identify the Volcano-like pattern.

3.6. Effect of the redissolution process on the quantification method

The redissolution process had no significant influence on the effective molar attenuation coefficient, but it had an effect on its uncertainty (Figure S21). Increasing the amount of DI water used in the redissolution from 5 mL to 10 mL, as well as filtering the redissolved solution with a 0.22 µm pore size syringe filter had no significant effect on the effective molar attenuation coefficient, suggesting that no insoluble ammonium salts remained after any of the considered redissolution processes. Storing the samples for 4 days (redissolution processes 3 to 5) presented larger uncertainties in the effective molar attenuation coefficient than the other redissolution processes, indicating that small amounts of TAN can be lost from some samples during the storage period, but that this loss is independent of the initial ammonia concentration. The fact that the redissolution process had no significant effect on the effective molar attenuation coefficient demonstrates that the redissolution process does not contribute meaningful to the loss of TAN and that the evaporation portion of the evaporation-redissolution process is primary responsible for ammonia losses.

The optimum redissolution process is to add 5 mL of freshly prepared DI water after cooling the sample and analyze the samples immediately. In the case that the sample presents some turbidity or solids in suspension, it should be filtered, since the solids may interfere with the UV-Visible measurement. Since no significant differences occurred due to filtering the sample (comparing redissolution processes 1 and 2), the sample can be filtered before analysis, with no additional loss or change to the quantification of TAN.

3.7. Reproducibility of the ammonia quantification method in non-aqueous samples

The experimental maximum absorbance-TAN concentration calibration curves obtained for THF-ethanol 99:1 vol.% 0.2 M $LiClO_4$ samples analyzed using the salicylate method for non-aqueous samples (section 2.3 and Figure S15), on different days did not present significant differences (Figure S22). This shows that the method proposed in this work for quantifying ammonia in non-aqueous samples is reproducible, since the obtained calibration curves are nearly identical day after day. The recommendation stated for the aqueous case in section 3.4., is also applicable to the non-aqueous case: even though it is not strictly necessary to include a calibration set in every batch of analyzed samples, it is advisable to do so. These calibration samples serve as validation of both the evaporation-redissolution process and the salicylate method, allowing for errors effecting the entire batch of samples to be easily identified.

4. Recommended method

The procedure presented here for ammonia quantification in non-aqueous samples is based on an evaporation-redissolution process (Figure 7). This process can introduce significant losses in the quantification method due to the evaporation of ammonia. These losses can be minimized by adding concentrated HCl to the sample prior to the evaporation process. There is an optimum HCl volume that maximizes the TAN detection following evaporation-redissolution which strongly depends on the exact evaporation experimental setup and therefore should be determined experimentally prior to analyzing samples for TAN quantification. Even with optimal HCl volume, the evaporation-redissolution process introduces ~30% losses in the quantification method, preventing aqueous calibration curves from being applied to non-aqueous samples. Fortunately, losses in the evaporation-redissolution process are reproducible (Figure S22) and do not alter the linearity of the obtained calibration curve (Figure 5). The proposed evaporation-redissolution process is only applicable to solvents that can be easily evaporated and do not decompose into amines or other interferents during the evaporation process. If the method is to be applied to solvents with low vapor pressures or that may decompose into interferents when heated, alternative evaporation procedures should be investigated, such as vacuum evaporation.

The proposed method is able to quantify ammonia in aqueous samples with pHs between 6.5 and 13.0. Sample pHs in this range do not significantly affect the quantification method since the alkaline citrate reagent serves to adjust the pH of the solution to its optimal value. However, for samples with pHs between 6.5 and 4.0, the alkaline citrate solution is not able to increase the reaction pH sufficiently, leading to decreased dye yield and a significant decrease of the effective molar attenuation coefficient. Finally for acidic samples with pH<4.0, the salicylate precipitates out of the solution as salicylic acid, almost completely inhibiting the color formation. The alkaline hypochlorite reagent should never be added to a sample in which salicylic acid has precipitated: since this is an indicator of low pH, and adding the alkaline hypochlorite reagent to a low pH sample produces toxic gases. Samples with pH<6.5 should be neutralized with NaOH prior to applying the salicylate method to ensure dye yield is not adversely influenced by the pH of the reaction solution or salicylic acid precipitation.

The indophenol-type dye on which the salicylate method is based, reaches its steady state value 45 minutes after the addition of the reagents and remains relatively stable for at least 5 hours after the addition of reagents. Consequently, as long as samples are measured in this time window, no special care has to be taken to ensure that all the samples have exactly the same development time. However, the indophenol-type dye is not stable over longer time scales, and the ammonia quantification error due to the dye decomposition can become very significant for times > 5 hours, preventing the re-measuring of samples at a later time.

Ambient ammonia levels can be corrected by using a sample with no added TAN as a blank and reference sample for the UV-Vis measurement. Furthermore, the blank sample, when measured against pure DI water, can be used to verify that the nitroprusside concentration and pH are in the correct range and can be used to estimate the ambient ammonia level. Performing this verification with every batch of samples allows errors from reagent preparation/addition or moderate to severe ammonia contamination of the entire batch to be detected.

Finally, the proposed methods exhibits good reproducibility for a given reagent brand when measured on different days, allowing a calibration curve measured on a previous day to be re-used. However, the reagent supplier has a significant effect on the calibration curve, requiring that a new calibration curve be obtained for every brand of reagent used. Although no differences were observed in this work between different lots of a given reagent from the same supplier, it is still advisable to obtain a new calibration curve when starting a new reagent lot as the origin of this reagent-dependence is not fully understood. Even though it is not strictly necessary to include a calibration set in every batch of analyzed samples, it is advisable to do so. These calibration samples can be used as validation samples to detect errors that effect an entire batch of samples, such as issues with the reagents.

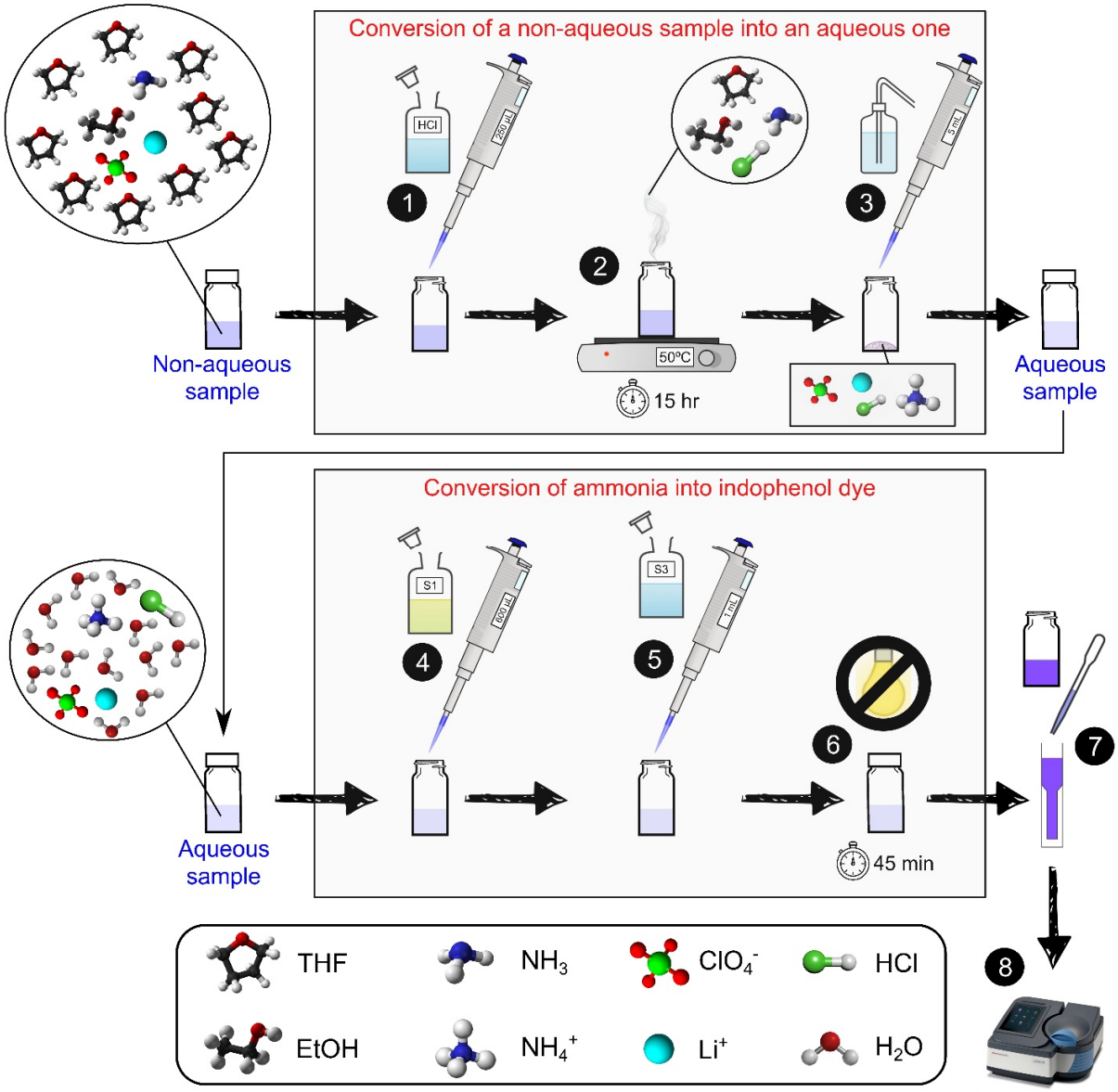

Figure 7. Ammonia quantification method proposed in this work for non-aqueous and aqueous samples. (1) Addition of concentrated hydrochloric acid. A part of the ammonia in the sample is lost during the evaporation process. There is an optimum HCl volume that minimizes the ammonia losses during the evaporation process, which strongly depends on the exact evaporation experimental setup. (2) Solvent evaporation. The solvent, and part of the ammonia and the HCl are evaporated out of the sample. (3) Redissolution process: Add 5 mL of freshly prepared Millipore® water after cooling the sample; and analyze immediately after the samples. In the case that the sample presents some turbidity, or solids in suspension, after introducing the water; it should be filtered. (4) Addition of the salicylate catalyst solution. If the sample has a pH below 4.0, the salicylate precipitates out of the solution as salicylic acid, nearly completely inhibiting the color formation in subsequent steps. The alkaline hypochlorite reagent should never be added to a sample in which salicylic acid has precipitated. (5) Addition of the alkaline hypochlorite solution. (6) Color development in the dark. Figure S5 displays the mechanism of the color formation reaction. If the sample has a pH below 6.5, the alkaline hypochlorite solution is not able to increase the reaction pH until its optimum value, which reduces the dye formation yield. If the sample contains Li^+ ions, these coordinate with the dye, reducing its intrinsic molar attenuation coefficient. (7) Sample loading into a cuvette. (8) UV-Visible spectrum measurement, from 850 nm to 350 nm with a step size of 0.5 nm and a sweep speed of 5 nm^{-1}.

5. Conclusions

In this work, the salicylate method was optimized for ammonia quantification in aqueous and non-aqueous samples, in the context of nitrogen electroreduction experiments. The proposed methods exhibit good reproducibility for a given reagent brand for both, aqueous and non-aqueous samples. Evaporation-redissolution allows a non-aqueous sample to be transformed into an aqueous sample, but the amount of ammonia lost due to evaporation is very sensitive to the amount of acid added (to convert NH_3 to NH_4^+) as well as any salt present in the sample, necessitating that calibration curves be obtained from standard solutions that exactly match the content of the non-aqueous electrolyte and are subjected to an identical evaporation-redissolution process. Aqueous samples with pHs between 6.5 and 13.0 can be measured directly, but samples with pHs below 6.5 need to be neutralized with NaOH prior to analysis, in order to avoid interference from suboptimal pH for the dye formation reaction or the precipitation of salicylic acid. Although the salicylate method can be highly sensitive to interferences from a wide variety of sources, with proper experimental controls, highly sensitive, accurate and reproducible results can be obtained.

Nomenclature

Roman symbols

A_λ	Absorbance at wavelength λ
A_λ^*	Normalized absorbance at wavelength λ
C	Molar concentration $(mol \cdot m^{-3})$
e	Relative quantification error
k	Reaction rate constant $\left(mol^{1-\alpha} \cdot m^{3(\alpha-1)} \cdot s^{-1}\right)$
K	Equilibrium constant
K_L	50%-velocity concentration Laidler kinetic parameter $(mol \cdot m^{-3})$
l	Optical path (m)
R^2	Determination coefficient
R	Pearson's correlation coefficient
r	Reaction rate $(mol \cdot m^{-3} \cdot s^{-1})$
r_{max}	Maximum-rate Laidler kinetic parameter $(mol \cdot m^{-3} \cdot s^{-1})$
t_{exp}	Expiry time (s)

Greek symbols

α	Reaction order
$\varepsilon^\star$	Effective molar attenuation coefficient $(m^3 \cdot mol^{-1} \cdot m^{-1})$
η	Loss factor
λ	Wavelength (m)
λ_{max}	Wavelength of the peak (m)
μ	Mean
σ	Standard deviation

Subscripts

TAN	Total ammonia nitrogen (i.e. $NH_3 + NH_4^+$)

Superscripts

$Final$	In the final mixture (i.e. after the reagent additions)
$Sample$	In the initial sample (i.e. before the reagent additions)

Author Contributions

Juan José Giner-Sanz: Conceptualization, Formal analysis, Investigation, Methodology, Writing the original draft, Review & editing. **Graham M. Leverick**: Conceptualization, Formal analysis, Investigation, Methodology, Validation, Writing the original draft, Review & editing. **V. Pérez-Herranz**: Funding acquisition, Methodology, Supervision, Writing the original draft, Review & editing. **Yang Shao-Horn**: Conceptualization, Funding acquisition, Methodology, Resources, Supervision, Writing the original draft, Review & editing.

Acknowledgments

This work was supported by the Toyota Research Institute through the Accelerated Materials Design and Discovery program. This work made use of the MRSEC Shared Experimental Facilities at MIT (SEM) supported by the National Science Foundation under award number DMR-1419807 as well as the HZDR Ion Beam Center TEM facilities. J.J.G.S. is very grateful to the Generalitat Valenciana and to the European Social Fund, for their economic support in the form of Vali+d postdoctoral grant (APOSTD-2018-001). G.M.L. was partially supported by a Natural Sciences and Engineering Research Council of Canada (NSERC) PGS-D and a Siebel Scholarship (Class of 2020).

References

[1] N. Gilbert, Dirt poor: the key to tackling hunger in Africa is enriching its soil. The big debate is about how to do it, Nature 483 (2012) 525-528.

[2] H. Liu, Ammonia synthesis catalyst 100 years: Practice, enlightenment and challenge, Chinese Journal of Catalysis 35 (2014) 1619-1640.

[3] V. Smil, Enriching the Earth: Fritz Haber, Carl Bosch, and the Transformation of World Food Production, Cambridge: MIT Press, 2004.

[4] Q. Wang, J. Guo and P. Chen, The Power of Hydrides, Joule 4 (2020) 705-709.

[5] J. Guo and P. Chen, Catalyst: NH_3 as an Energy Carrier, Chem 3 (2017) 709-712.

[6] J. Choi, B. Suryanto, D. Wang, H. Du, R. Hodgetts, F. Vallana, D. MacFarlane and A. Simonov, Identification and elimination of false positives in electrochemical nitrogen reduction studies, Nature Communications 1 (2020) 1-10.

[7] L. Wang, M. Xia, H. Wang, K. Huang, C. Qian, C. Maravelias and G. Ozin, Greening ammonia toward the solar ammonia refinery, Joule 2 (2018) 1055-1074.

[8] A. Medford and M. Hatzell, Photon-driven nitrogen fixation: current progress, thermodynamic considerations, and future outlook, ACS Catalysis 7 (2017) 2624-2643.

[9] J. Erisman, M. Sutton, J. Galloway, Z. Klimont and W. Winiwarter, How a century of ammonia synthesis changed the world, Nature Geoscience 1 (2008) 636-639.

[10] L. Winter, B. Ashford, J. Hong, A. Murphy and J. Chen, Identifying surface reaction intermediates in plasma catalytic ammonia synthesis., ACS Catalysis 10 (2020) 14763-14774.

[11] Q. Wang, J. Guo and P. Chen, Recent progress towards mild-condition ammonia synthesis, Journal of Energy Chemistry 36 (2019) 25-36.

[12] C. Van der Ham, M. Koper and D. Hetterscheid, Challenges in reduction of dinitrogen by proton and electron transfer, Chemical Society Reviews 43 (2014) 5183-5191.

[13] P. Wang, F. Chang, W. Gao, J. Guo, G. Wu, T. He and P. Chen, Breaking scaling relations to achieve low-temperature ammonia synthesis through LiH-mediated nitrogen transfer and hydrogenation, Nature Chemistry 9 (2017) 64-70.

[14] V. Kyriakou, I. Garagounis, A. Vourros, E. Vasileiou and M. Stoukides, An electrochemical haber-bosch process, Joule 4 (2020) 142-158.

[15] B. Suryanto, H. Du, D. Wang, J. Chen, A. Simonov and D. MacFarlane, Challenges and prospects in the catalysis of electroreduction of nitrogen to ammonia, Nature Catalysis 2 (2019) 290-296.

[16] M. Shipman and M. Symes, Recent progress towards the electrosynthesis of ammonia from sustainable resources, Catalysis Today 286 (2019) 57-68.

[17] C. Fernandez and M. Hatzell, Economic considerations for low-temperature electrochemical ammonia production: Achieving Haber-Bosch parity, Journal of the Electrochemical Society 167 (2020) 143504.

[18] A. Tricker, K. Hebisch, M. Buchmann, Y. Liu, M. Rose, E. Stavitski, A. Medford, M. Hatzell and C. Sievers, Mechanocatalytic ammonia synthesis over TiN in transient microenvironments, ACS Energy Letters 5 (2020) 3362-3367.

[19] N. Morlanés, S. Katikaneni, S. Paglieri, A. Harale, B. Solami, S. Sarathy and J. Gascon, Technological Roadmap to the Ammonia Energy Economy: Current State and Missing Technologies, Chemical Engineering Journal 408 (2020) 127310.

[20] D. MacFarlane, P. Cherepanov, J. Choi, B. Suryanto, R. Hodgetts, J. Bakker, F. Vallana and A. Simonov, A Roadmap to the Ammonia Economy, Joule 4 (2000) 1186-1205.

[21] Y. Wang, M. Shi, D. Bao, F. Meng, Q. Zhang, Y. Zhou, K. Liu, Y. Zhang, J. Wang, Z. Chen and J. Chen, Generating Defect-Rich Bismuth for Enhancing the Rate of Nitrogen Electroreduction to Ammonia, Angewandte Chemie International Edition 58 (2019) 9464-9469.

[22] X. Guo, J. Gu, S. Lin, S. Zhang, Z. Chen and S. Huang, Tackling the Activity and Selectivity Challenges of Electrocatalysts toward the Nitrogen Reduction Reaction via Atomically Dispersed Biatom Catalysts, Journal of the American Chemical Society 142 (2020) 5709-5721.

[23] L. Shi, Y. Yin, S. Wang, X. Xu, H. Wu, J. Zhang, S. Wang and H. Sun, Rigorous and reliable operations for electrocatalytic nitrogen reduction, Applied Catalysis B: Environmental 278 (2020) 119325.

[24] S. Andersen, V. Čolić, S. Yang, J. Schwalbe, A. Nielander, J. McEnaney, K. Enemark-Rasmussen, J. Baker, A. Singh, B. Rohr, M. Statt, S. Blair, S. Mezzavilla, J. Kibsgaard, P. Vesborg, M. Cargnello and et. al., A rigorous electrochemical ammonia synthesis protocol with quantitative isotope measurements, Nature 570 (2019) 504-508.

[25] F. Koch and T. McMeekin, A new direct nesslerization micro-Kjeldahl method and a modification of the Nessler-Folin reagent for ammonia, Journal of the American Chemical Society 46 (1924) 2066-2069.

[26] I. Ivančič and D. Degobbis, An optimal manual procedure for ammonia analysis in natural waters by the indophenol blue method, Water Research 18 (1984) 1143-1147.

[27] A. LeDuy and R. Samson, Testing of an ammonia ion selective electrode for ammonia nitrogen measurement in the methanogenic sludge, Biotechnology Letters 4 (1982) 303-306.

[28] M. Rey, High-capacity cation-exchange column for enhanced resolution of adjacent peaks of cations in ion chromatography, Journal of Chromatography A 920 (2001) 61-68.

[29] G. Duan, Y. Ren, Y. Tang, Y. Sun, Y. Chen, P. Wan and X. Yang, Improving the Reliability and Accuracy of Ammonia Quantification in Electro-and Photochemical Synthesis, ChemSusChem 13 (2020) 88-96.

[30] J. McEnaney, A. Singh, J. Schwalbe, J. Kibsgaard, J. Lin, M. Cargnello, T. Jaramillo and J. Nørskov, Ammonia synthesis from N2 and H2O using a lithium cycling electrification strategy at atmospheric pressure, Energy & Environmental Science 10 (2017) 1621-1630.

[31] J. Liu, M. Kelley, W. Wu, A. Banerjee, A. Douvalis, J. Wu, Y. Zhang, G. Schatz and M. Kanatzidis, Nitrogenase-mimic iron-containing chalcogels for photochemical reduction of dinitrogen to ammonia, Proceedings of the National Academy of Sciences 113 (2016) 5530-5535.

[32] C. Fernandez, N. Hortance, Y. Liu, J. Lim, K. Hatzell and M. Hatzell, Opportunities for intermediate temperature renewable ammonia electrosynthesis, Journal of Materials Chemistry A 8 (2020) 15591.

[33] Y. Zhao, R. Shi, X. Bian, C. Zhou, Y. Zhao, S. Zhang, F. Wu, G. Waterhouse, L. Wu, C. Tung and T. Zhang, Ammonia Detection Methods in Photocatalytic and Electrocatalytic Experiments: How to Improve the Reliability of NH3 Production Rates?, Advanced Science 6 (2019) 1802109.

[34] M. P. E. Berthelot, Violet d'aniline, Répertoire de Chimie Appliquée 1 (1859) 284.

[35] Y. Song, D. Johnson, R. Peng, D. Hensley, P. Bonnesen, L. Liang, J. Huang, F. Yang, F. Zhang, R. Qiao, A. Baddorf, T. Tschaplinski, N. Engle, M. Hatzell, Z. Wu, D. Cullen, H. Meyer III, B. Sumpter and A. Rondinone, A physical catalyst for the electrolysis of nitrogen to ammonia, Science Advances 4 (2018) 1700336.

[36] M. Prieto-Blanco, A. Ballester-Caudet, F. Souto-Varela, P. López-Mahía and P. Campíns-Falcó, Rapid evaluation of ammonium in different rain events minimizing needed volume by a cost-effective and sustainable PDMS supported solid sensor, Environmental Pollution 265 (2020) 114911.

[37] M. Prieto-Blanco, N. Jornet-Martinez, J. Verdú-Andrés, C. Molíns-Legua and P. Campíns-Falcó, Quantifying both ammonium and proline in wines and beer by using a PDMS composite for sensoring, Talanta, 198 (2019) 371-376.

[38] M. Prieto-Blanco, N. Jornet-Martínez, Y. Moliner-Martínez, C. Molins-Legua, R. Herráez-Hernández, J. Verdú-Andrés and P. Campins-Falcó, Development of a polydimethylsiloxane–thymol/nitroprusside composite based sensor involving thymol derivatization for ammonium monitoring in water samples, Science of the Total Environment 503 (2015) 105–112.

[39] H. Verdouw, C. Van Echteld and E. Dekkers, Ammonia determination based on indophenol formation with sodium salicylate, Water Research 12 (1978) 399-402.

[40] A. Cerda, M. Oms, R. Forteza and V. Cerda, Evaluation of flow injection methods for ammonium determination in wastewater samples, Analytica Chimica Acta 311 (1995) 165-173.

[41] C. Molins-Legua, S. Meseguer-Lloret, Y. Moliner-Martinez and P. Campíns-Falcó, A guide for selecting the most appropriate method for ammonium determination in water analysis, Trends in Analytical Chemistry 25 (2006) 282-290.

[42] A. Kempers and C. Kok, Re-examination of the determination of ammonium as the indophenol blue complex using salicylate, Analytica Chimica Acta 221 (1989) 147-155.

[43] M. Weatherburn, Phenol-hypochlorite reaction for determination of ammonia, Analytical Chemistry 39 (1967) 971-974.

[44] R. Willis, M. Montgomery and P. Allen, Improved method for manual, colorimetric determination of total Kjeldahl nitrogen using salicylate, Journal of Agricultural and Food Chemistry 44 (1996) 1804-1807.

[45] F. Jüttner, Interference with ammonium determination by the indophenol-type reaction of salicylate and dichloroisocyanurate, Fresenius' Journal of Analytical Chemistry 363 (1999) 128-129.

[46] J. Giner-Sanz, G. Leverick, V. Perez-Herranz and Y. Shao-Horn, Salicylate Method for Ammonia Quantification in Nitrogen Electroreduction Experiments: The Correction of Iron III Interference, Journal of the Electrochemical Society 167 (2020) 134519.

[47] L. Zhou and C. Boyd, Comparison of Nessler, phenate, salicylate and ion selective electrode procedures for determination of total ammonia nitrogen in aquaculture, Aquaculture 450 (2016) 187-193.

[48] C. Bower and T. Holm-Hansen, A salicylate-hypochlorite method for determining ammonia in seawater, Canadian Journal of Fisheries and Aquatic Sciences 37 (1980) 794-798.

[49] P. Le and C. Boyd, Comparison of phenate and salicylate methods for determination of total ammonia nitrogen in freshwater and saline water, Journal of the World Aquaculture Society 43 (2012) 885-889.

[50] P. Searle, The Berthelot or indophenol reaction and its use in the analytical chemistry of nitrogen. A review, Analyst 109 (1984) 549-568.

[51] N. Lazouski, Z. Schiffer, K. Williams and K. Manthiram, Understanding continuous lithium-mediated electrochemical nitrogen reduction, Joule 3 (2019) 1127-1139.

[52] A. Fraser and J. Russell, A spectrophotometric method for determination of cation-exchange capacity of clay minerals, Clay Minerals 8 (1969) 229-230.

[53] M. Krom, Spectrophotometric determination of ammonia: a study of a modified Berthelot reaction using salicylate and dichloroisocyanurate, Analyst 105 (1980) 305-316.

[54] D. Lide, CRC Handbook of Chemistry and Physics, 85th edition ed., Boca Ratón: CRC Press, 2005.

[55] Z. Qiang and C. Adams, Determination of monochloramine formation rate constants with stopped-flow spectrophotometry, Environmental Science & Technology 38 (2004) 1435-1444.

[56] I. Weil and J. Morris, Kinetic studies on the chloramines. I. The rates of formation of monochloramine, N-chlormethylamine and N-chlordimethylamine, Journal of the American Chemical Society 71 (1949) 1664-1671.

[57] J. Harwood and A. Kuhn, A colorimetric method for ammonia in natural waters, Water Research 4 (1970) 805-811.

[58] M. Liddicoat, S. Tibbitts and E. Butler, The determination of ammonia in natural waters, Water Research 10 (1976) 567-568.

[59] R. Pym and P. Milham, Selectivity of reaction among chlorine, ammonia, and salicylate for determination of ammonia, Analytical Chemistry 48 (1976) 1413-1415.

[60] R. Every-Pym and P. Mllham, Selectivity of Reaction among Chlorine, Ammonia, and Salicylate for Determination of Ammonia, Analytical Chemistry 48 (1976) 1413-1415.

[61] A. Tsuneto, A. Kudo and T. Sakata, Lithium-mediated electrochemical reduction of high pressure N_2 to NH_3, Journal of Electroanalytical Chemistry 367 (1994) 183-188.

[62] C. Cragoe, C. Meyers and C. Taylor, The vapor pressure of ammonia, Journal of the American Chemical Society 42 (1920) 206-229.